Electronic Supplementary Information

Superwetting Photothermal CuS@SiO_2 Nanocomposites for Anti-/de-icing and Synchronous Water Evaporation and Photodegradation of Dyes

Rong Zhang[a], Helong Zhang[a], Yuwei Zhong[a], Shouqin Tian[a], Xiong Qian[b], Lee Li[c], Javad Shabani Shayeh[d], Roya Sedghi[d], Xiujian Zhao[a], Yi Xie[a,*]

[a] *State Key Laboratory of Silicate Materials for Architectures, Wuhan University of Technology, No. 122, Luoshi Road, Wuhan 430070, P. R. China.*

[b] *Department of Civil and Environment Engineering, and Research Centre for Resources Engineering towards Carbon Neutrality, The Hong Kong Polytechnic University, Hong Kong, China.*

[c] *School of Electrical and Electronic Engineering, Huazhong University of Science and Technology (HUST), Wuhan 430074, China.*

[d] *Protein Research Center, Shahid Beheshti University, G. C., Velenjak, Tehran, Iran.*

Corresponding Author:

E-mail: xiey@whut.edu.cn

Contents

1. Experimental section

Materials and reagents. Copper acetate monohydrate ($C_4H_6CuO_4 \cdot H_2O$, 99.95%), hexamethyldisilazane (HMDS, AR), butyl acetate (AR) and NaOH (96.0%) were purchased from Aladdin. Methyl orange ($C_{14}H_{14}N_3NaO_3S$, MO), methylene blue ($C_{16}H_{18}ClN_3S \cdot 3H_2O$, MB), octadecene (ODE, 90%), oleylamine (OM, 80-90%) and hydroxy acrylic resin (HAR) were achieved from Macklin, toluene (anhydrous, 99.8%) and elemental sulfur (99%) from Strem Chemicals, Rhodamine B ($C_{28}H_{31}ClN_2O_3$, RhB, AR) from Tianjin Kermel Chemical Reagent Co. Ltd., ethanol (EtOH, AR) and tetraethyl orthosilicate (TEOS, AR) from Sinopharm Chemical Reagent Co. Ltd. Alkyd resin and polypropylene were acquired from Shenzhen Yoshida Chemical Co. Ltd., nylon powder (500 #) from DuPont, and tetrafluoro resin (HLR-6) from Shanghai East Fluorochemical Technology Co. Ltd. All chemicals were used as received without any further purification.

Synthesis of covellite (CuS) nanoplates. Covellite (CuS) nanoplates were synthesized by applying minor modifications to a previously reported procedure. In short, an orange-red sulfur solution was prepared by degassing a mixture of 0.256 g (8 mmol) of sulfur, 40 mL of ODE and 10 mL of OM in a 100 mL three-neck flask at 90 ^oC under vacuum for 30 min. The sulfur solution was cooled to room temperature (RT) in an argon atmosphere, then 0.798 g (4.0 mmol) of copper(II) acetate monohydrate was added. Next, the solution was degassed at RT for 30 min, then heated up to 200 ^oC (with a ramp of 8-10 ^oC/min) and kept at this temperature for 30 min. The resulting solution was collected after it had been cooled to RT. The nanoplates were precipitated and cleaned with methanol, and were finally dispersed in 10 mL toluene for the subsequent preparation of CuS@SiO_2 nanocomposites. The precipitated CuS nanoplates were finally dispersed in 10 mL toluene for the subsequent preparation of CuS@SiO_2 nanocomposites.

Synthesis of CuS@SiO_2 nanocomposites and the surface modification. The synthesis of CuS@SiO_2 core-shell nanocomposites was realized by hydrolysis of TEOS

in the presence of CuS nanoparticle (NP) dispersions. In a typical synthesis, 5 mL ethanol was added into 1.2 mL of the as-prepared CuS nanoparticle (NP) dispersions. Then, 0.3 mL NaOH (1.8 M, distilled H_2O as solvent) was added in the CuS dispersions under stirring, followed by addition of 1 mL TEOS. The reaction was then kept for 24 h to obtain the hydroxyl-modified CuS@SiO_2 nanocomposites, which are used for the subsequent fabrication of superhydrophilic (SHI) coatings. The surface wettability of the CuS@SiO_2 coatings can be tuned by changing the amount of HMDS that introduced for surface modification. In a typical fabrication of superhydrophobic CuS@SiO_2 coating, 0.6 mL HMDS was added in the hydroxyl-modified CuS@SiO_2 dispersions and the reaction was kept for 6 h, leading to the formation of methyl-modified CuS@SiO_2 nanocomposites.

Fabrication of photothermal CuS@SiO_2-incorporated melamine foam for water evaporation and photocatalytic dyes degradation. The photothermal CuS@SiO_2-incorporated melamine foam (MF) with SH-SHI Janus wettability was fabricated by spray depositing the methyl-modified CuS@SiO_2 nanocomposites on one side of the foam (labelled as top side) followed by immersing another side of the foam (labelled as bottom side) in a hydroxyl-modified CuS@SiO_2 dispersion (2.5 mL). The sample was then dried at RT for 24 h for the subsequent characterizations, photocatalysis and water evaporation. For comparison, a fully SHI photothermal MF was obtained by dipping both sides into a dispersion of hydroxyl-modified CuS@SiO_2 nanocomposite. The fully SH photothermal MF was fabricated by spray depositing methyl-modified CuS@SiO_2 on both sides of the MF. The spray-coating process was carried out by using an airbrush with a nozzle diameter of 1.0 mm under an air pressure of 2.0-2.5 bar (nozzle to foam surface distance: 15-20 cm).

Fabrication of superhydrophobic photothermal CuS@SiO_2 coatings for anti-/de-icing. In our work, the resin-based dispersion and the methyl-modified CuS@SiO_2 suspension were used as primer and topcoat, respectively, to fabricate SH photothermal coatings for anti-/de-icing. Two cycles of spraying were performed for both primer and topcoat under ambient environment (20-30^{o}C, relative humidity ~50-60 %). The resin-

based dispersions were prepared by mixing several resins in butyl acetate. Typically, hydroxylated acrylic resin (9 g) was dispersed in butyl acetate (30 mL) under stirring, followed by sequentially adding alkyd resin (4.0 g), polypropylene (1.2 g), tetrafluoro resin (1.5 g), KH550 solution (0.3 mL, pre-dissolved 0.12 mL KH550 in 0.18 ml H_2O) and nylon powder (1.0 g). The mixtures were then stirred for 12 h to obtain the resin dispersions, which is used for fabricating primer. The airbrush with a nozzle diameter of 1.0 mm at a pressure of 2.0-2.5 bar (nozzle to substrate surface distance 15-20 cm) was used for spraying. The resin-based primer layer was kept for evaporation for 2 min before depositing the SH topcoat by spraying the methyl-modified CuS@SiO_2 suspension. After spraying, the coatings were dried at RT for 24 h for subsequent characterization and test. Pre-cleaned glass slides (10.0 × 5.0 cm) were used as substrates.

Characterizations. The transmission electron microscopy (TEM) and high-resolution TEM (HRTEM) measurements were performed on a JEM 2100F (JEOL, Japan) microscope equipped with a field emission gun working at 200 kV accelerating voltage. The samples were prepared by drop-casting the diluted nanoparticle solutions on the 300 mesh Cu grids covered with ultrathin amorphous carbon film, which were then placed in a high vacuum pumping station to let the solvent evaporate completely and to prevent oxidation. The phase and lattice parameter were analyzed by testing powder samples on a Bruker D8 Advanced X-ray diffractometer (XRD) equipped with a 1.8 kW CuKα ceramic X-ray tube, operating at 40 kV and 40 mA. XRD data analysis was performed using X'PertHighScore plus software from PANalytical. The surface morphologies of the various coatings were investigated using a field emission scanning electron microscopy (FESEM, Hitachi S-4800) by keeping the scan rate of 256 Hz. Fourier transform infrared (FTIR) (Nicolet 6700, USA) spectra test was performed from 4000 to 400 cm^{-1} to analyze the surface chemical structure of the coatings. The UV-Vis-NIR optical absorption spectra of the methyl-modified CuS@SiO_2 nanocomposites were recorded using a UV-Vis-NIR spectrophotometer (UV-3600) in the 350-2000 nm range, by using ethanol as solvent. The diluted NP solutions were

prepared in 1 cm path length quartz cuvettes with airtight screw caps. The static water contact angle (WCA) was measured on an optical contact angle goniometer (Theta Lite, Biolin Scientific) via the sessile drop technique at RT. The volumes of the water droplets for the WCA measurements were 10 μL.

Simulated solar-driven evaporation experiments and the evaporation efficiency (η) calculation. The simulated solar evaporation experiments were carried out at room temperature and a RH of 55 ± 5%. In the present work, we used a xenon lamp (CEL-S500-T5) to simulate sunlight for water evaporation experiments. In the water evaporation case, CuS@SiO_2-incorporated MF (2.5 cm × 2.5 cm × 0.5 cm) was horizontally floated on the simulated seawater containing NaCl (3.5 - 10 wt%) in a 50 mL glass beaker. The light source was located exactly above the MF surface with a distance of 15 cm. A solar power meter (CEL-S500-T5, Beijing China Education Au-light Technology) was used to check the illumination intensity, and the light intensity could vary from 0 to 2 sun (1 sun equals 100 mW cm^{-2}). The photothermal conversion performance of the materials was evaluated by monitoring the surface temperature evolution of specimens and the weight loss of the water, which were recorded using an infrared thermal imager (FLIR E6-xt) and a digital balance (ATX-224, Shimadzu Corporation) with an accuracy of 0.1 mg, respectively.

Photothermal water evaporation efficiency (η) can be calculated according to the following Equation:

$$\eta = 1 - \Phi - Q_1 - Q_2 \quad (1)$$

where Φ, Q_1 *and* Q_2 denote the heat flux (W), the convective heat energy and the conduction heat energy, respectively, which can be calculated according to the previously-reported Equations [1].

Synchronous photocatalytic dyes degradation and water evaporation. The photocatalytic activity of the CuS@SiO_2-incorporated MF was evaluated by the photodegradation of dyes such as MB, MO and RhB in a simulated seawater. The light source and irradiation parameters are the same as those in solo water evaporations as-

mentioned above. Briefly, CuS@SiO_2-incorporated MF was floated on the surface of simulative dye-polluted seawater (50 mL) with 5 mg L^{-1} of dye and salinity of 3.5 wt% (NaCl). The water evaporation rate was evaluated for the simulative dye-polluted seawater (The solution was stirred for 30 min in the dark to achieve an adsorption-desorption equilibrium between dye and the photocatalyst, followed by exposing the system to sunlight simulator. At various time intervals, 2.5 mL dye solution was taken out to record the UV-visible absorption spectra. The photodegradation efficiency (%) of dyes was calculated by the following equation:

$$\text{Degradation (\%)} = ((C_0\text{-}C_t)/C_0) \text{ X } 100\% = ((A_0\text{-}A_t)/A_0) \text{ X } 100\% \quad (2)$$

where C_0 and C_t represent the initial concentration and instant concentration of dyes at photodegradation time, A_0 and A_t represent the corresponding absorbance intensity of dyes .

The experimental data photocatalysis were applicable to pseudo-first-order kinetic model as below:

$$-\ln(A_t/A_0) = -\ln(C_t/C_0) = kt \quad (3)$$

where k represents the rate constant.

Anti-icing/deicing test. The anti-/de-icing experiments were conducted on a home-made setup, which consists of a sunlight simulator, a cooling stage, and an infrared thermal imager (FLIR E6-xt). The surfaces of the samples were illuminated with the simulated sunlight whose light intensity could vary from 0.1 to 2 sun. The surface temperature evolution of samples was recorded using a thermal imager. The freezing time of water droplets (60 μL, dyed by MB) on the various coatings (i.e., noncoated glass slide, CuS@SiO_2 SH coating, SiO_2 SH coating, resin-based hydrophobic coating) was recorded at different temperatures and under simulated sunlight ranging from 0.1 to 2.0 sun. The photothermal de-icing experiment was conducted by monitoring the melting process under simulated solar irradiation. The ice pillar was frozen on the coating surface, and the specimen together the setup was tilted to 30° and the temperature was then fixed to -15°C. Both the freezing and the photothermal heating

processes including the melting of ice were recorded using a digital camera under the simulated solar illumination.

2. Characterization of the as-synthesized CuS nanoplates, CuS@SiO_2 nanocomposite, and CuS@SiO_2-incorporated MF

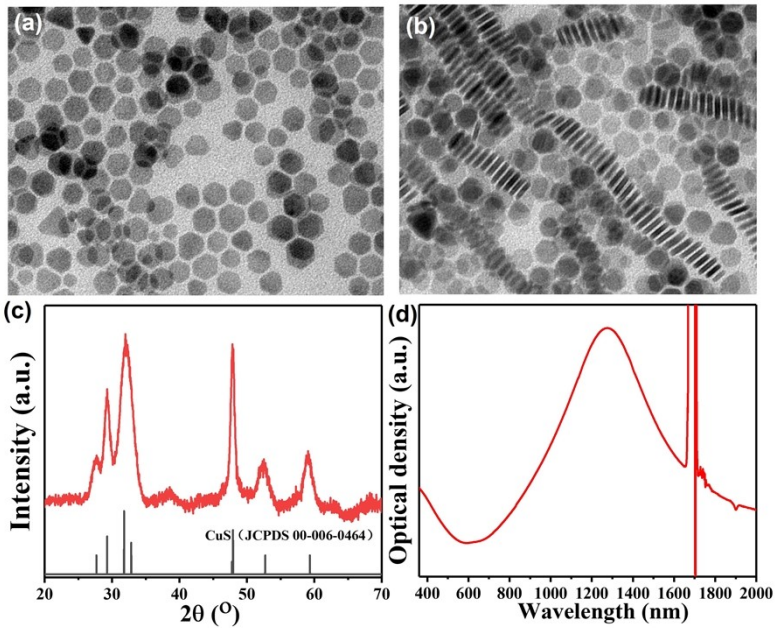

Fig. S1. TEM images (a-b), and XRD pattern (c), and absorption spectrum (d) of the as-synthesized CuS nanoplates. The experimental XRD peaks observed at two theta of 27.7°, 29.3°, 31.9°, 48.0°, 52.7° and 58.7° of the NCs can be respectively indexed to the diffraction planes of (101), (102), (103), (110), (108) and (203) of covellite phase (JCPDS No. 00-006-0464), which is in good agreement with the experimental XRD analysis of covellite CuS nanocrystals [2-4].

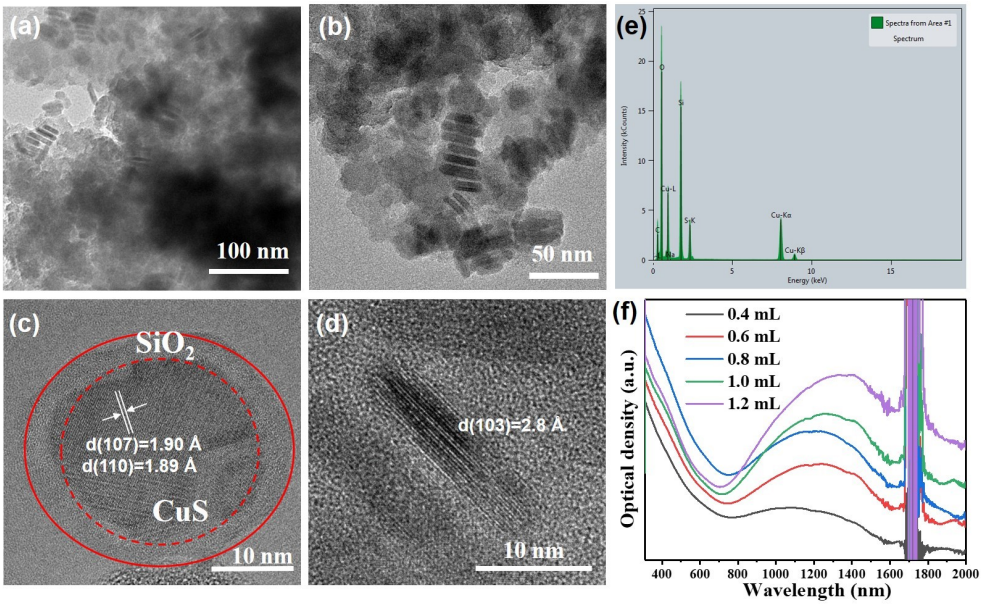

Fig. S2. TEM images (a-b), HRTEM images (c-d), and EDS spectrum (e) of the representative CuS@SiO_2 nanocomposites as-synthesized with 1.2 mL of CuS dispersion. (f) UV-vis absorption spectra of the CuS@SiO_2 nanocomposites collected in the presence of different amounts of CuS nanoparticle dispersion.

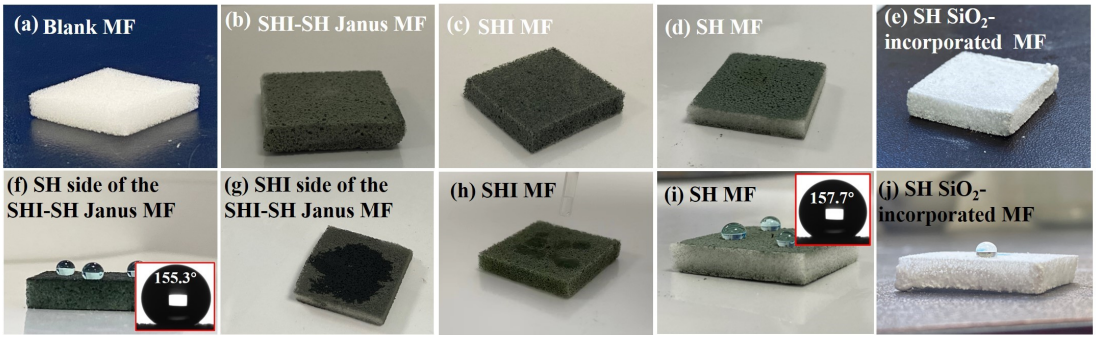

Fig. S3. (a-d) Digital photographs of the blank melamine foam (MF) (a), and various as-synthesized CuS@SiO_2-incorporated MFs. (e-h) Digital photographs of the various as-synthesized CuS@SiO_2-incorporated MFs together with methylene blue-dyed water droplets on the surface. Insets in panels e) and h) show the water contact angle images of the corresponding SH surfaces.

3. **Interfacial solar-driven photothermal simulated seawater evaporation**

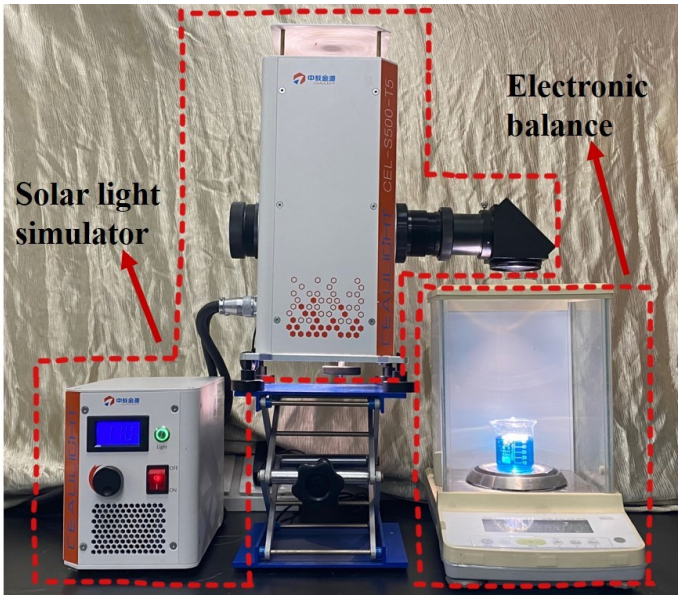

Fig. S4. Photographs of the lab-made indoor device for synchronous solar-driven photocatalytic dyes degradation and seawater evaporation.

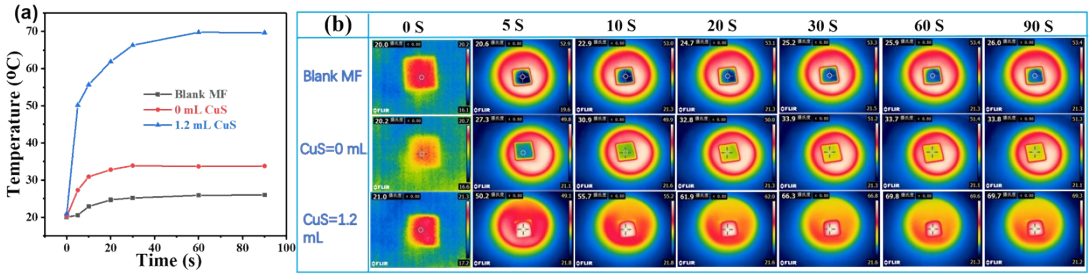

Fig. S5. Surface temperature curves (a) and Infrared images (b) of the different MFs under 1.0 sun irradiation.

Table S1. Performance comparison of the CuS@SiO_2 composite in this work with other previously reported materials under 1 sun illumination.

Researchers	Materials	Solar intensity (kW m^{-2})	Evaporation efficiency (%)	Evaporation rate (kg m^{-2} h^{-1})
Wang et al. [5]	WO_3/Ag/PbS	1	94	1.90
Zhang et al.[6]	PANI/DE@PVA/MF	1	95	1.689
Yang et al.[7]	Ag-PDA@wood	1	88.6	1.58
Wang et al. [8]	Porous carbon /polyaniline foam	1	87.3	1.496
Zhao et al.[9]	PDA@MXene photothermal membrane	1	85.2	1.276
Yang et al. [10]	MoS_2 and MXene composite aerogel	1	96.58	2.75
Zhang et al. [11]	MXene on lignin-cellulosic sponges	1	95.5	2.48
Xu et al. [12]	Cu_3BiS_3@V_2C/BF membrane	1	88.4	1.68
Kang et al. [13]	Au@$Cu_{2-x}S$ hybrids bonded $Ti_3C_2T_x$	1	96.1%	2.023
Wang et al. [14]	PDA/PU Janus evaporator	1	90.67	1.26
Chen et al. [15]	Janus wood evaporators	1	92.3	1.35
Chang et al. [16]	graphene oxide foam	1	89.6	1.43
Liu et al. [17]	$Ti_3C_2T_X$/carbon aerogels	1	92.3	1.48

Ming et al. [18]	MXene/graphene oxide aerogel	1	90.7	1.27
Wang et al. [19]	porous carbon/polyaniline	1	87.3	1.496
Yang et al. [20]	$Cu_2SnSe_3/Cu_2ZnSnSe$ cellulose membrane	1	86.6	1.657
This work	CuS@SiO_2 composite	1	89.16	1.962
This work	CuS@SiO_2 composite	1.5	89.70	2.76
This work	CuS@SiO_2 composite	2.0	90.35	3.408

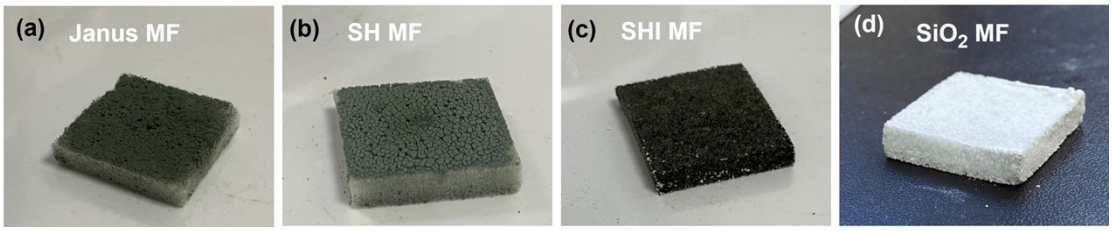

Fig. S6. Digital photographs of the various samples after running evaporation and drying at room temperature: (a) Janus CuS@SiO_2-incorporated MF, (b) fully SH CuS@SiO_2-incorporated MF, (c) fully SHI CuS@SiO_2-incorporated MF, and (d) Janus SiO_2-incorporated MF.

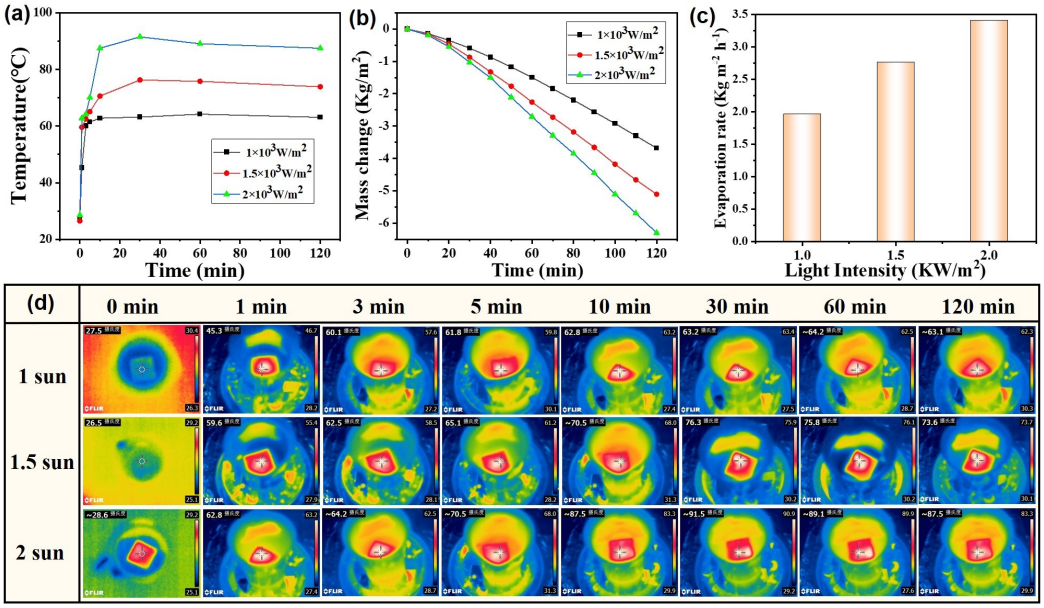

Fig. S7. (a) Surface temperature under different irradiation intensity in the presence of the CuS@SiO_2-incorporated MF with Janus wettability. (b-c) Mass reduction of water and evaporation rates for simulated seawater under different irradiation intensity. (d) Infrared images of the CuS@SiO_2-incorporated MF under different irradiation intensity.

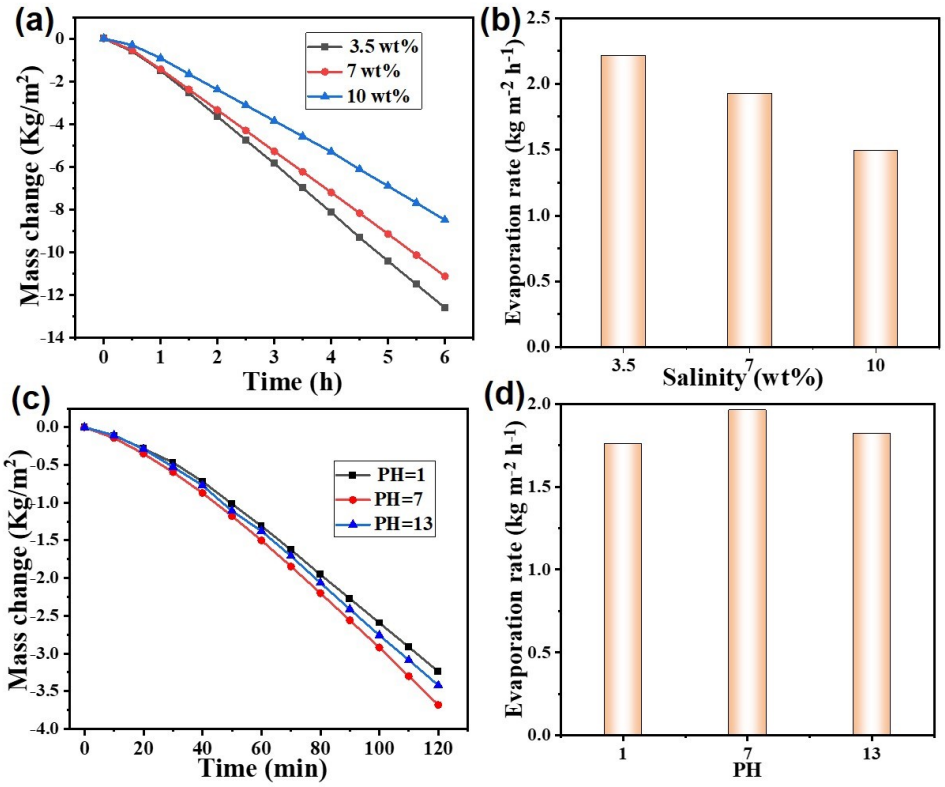

Fig. S8. The mass reduction of water (a,c) and evaporation rates (b,d) for simulated seawater with different salinity (a,b) and pH values (c-d) under 1 sun illumination in the presence of CuS@SiO_2 evaporator with Janus wettability.

4. Solar-driven dyes degradation and mechanism

Eqns. (1)-(7) illustrate the photodegradation mechanism in the presence of $CuS@SiO_2$ and H_2O_2. Through simulated solar irradiation, the CuS component in the $CuS@SiO_2$ nanocomposite induce electrons (e^-) and holes (h^+). These photo-excited e^- and h^+ can transfer to the surface of the $CuS@SiO_2$ nanocomposite, and react with oxidants and reductants to form $\cdot O_2^-$ and hydroxyl radicals ($\cdot OH$). Dyes molecules can be then decomposed through an oxidation reaction by the as-formed $\cdot O_2^-$ and $\cdot OH$. The photo-induced e^- and h^+ might recombine in the absence of related traps, resulting in decreasing photocatalytic activity. The presence of H_2O_2 can significantly minimize the recombination of e^- and h^+, and consequently enhances the photodegradation efficiency.

$$CuS@SiO_2 + h\nu \rightarrow h^+ (CuS@SiO_2) + e^- (CuS@SiO_2) \quad (1)$$

$$e^- (CuS@SiO_2) + O_2 \rightarrow {}^{\bullet}O_2^- \quad (2)$$

$$h^+ (CuS@SiO_2) + OH^- \rightarrow {}^{\bullet}OH \quad (3)$$

$$e^- (CuS@SiO_2) + H_2O_2 \rightarrow {}^{\bullet}OH + OH^- \quad (4)$$

$$h^+ (CuS@SiO_2) + H_2O_2 \rightarrow {}^{\bullet}OOH + H^+ \quad (5)$$

$${}^{\bullet}OOH \rightarrow {}^{\bullet}O_2^- + H^+ \quad (6)$$

$$\text{Dyes} + {}^{\bullet}OH + {}^{\bullet}O_2^- \rightarrow \text{degradation products} \quad (7)$$

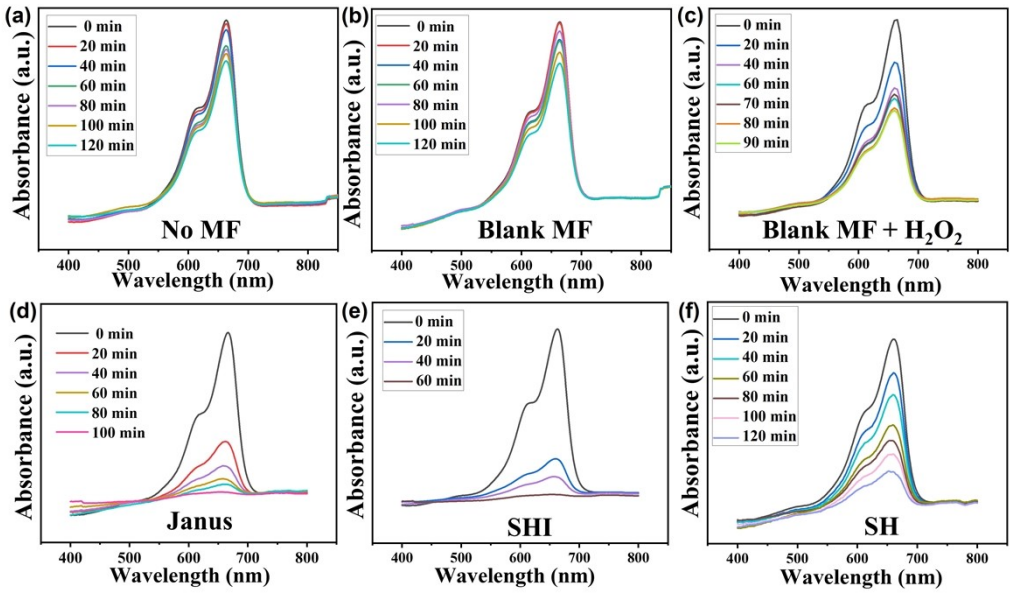

Fig. S9. (a-c) Evolution of the UV-vis absorption spectra of MB during photocatalytic degradation in the absence of photocatalysts and foam (a), in the presence of blank foam alone (b) and both blank foam and H_2O_2 (c). (d-f) Evolution of the UV-vis absorption spectra of MB during photocatalytic degradation in the presence of the various self-floated foam photocatalysts as dictated.

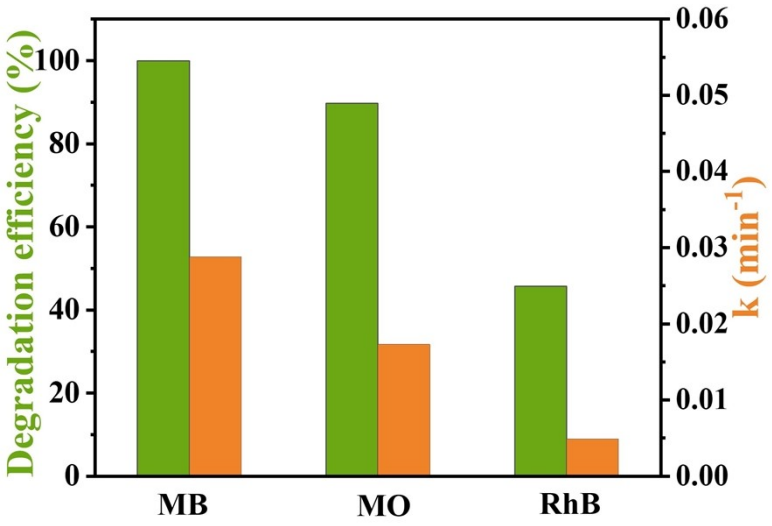

Fig. S10. Degradation efficiency and apparent rate constant of the various dyes in 120 min with Janus CuS@SiO_2-incorporated MFs as photocatalysts under 1.0 sun illumination.

5. **Anti-icing/deicing performances of various coatings**

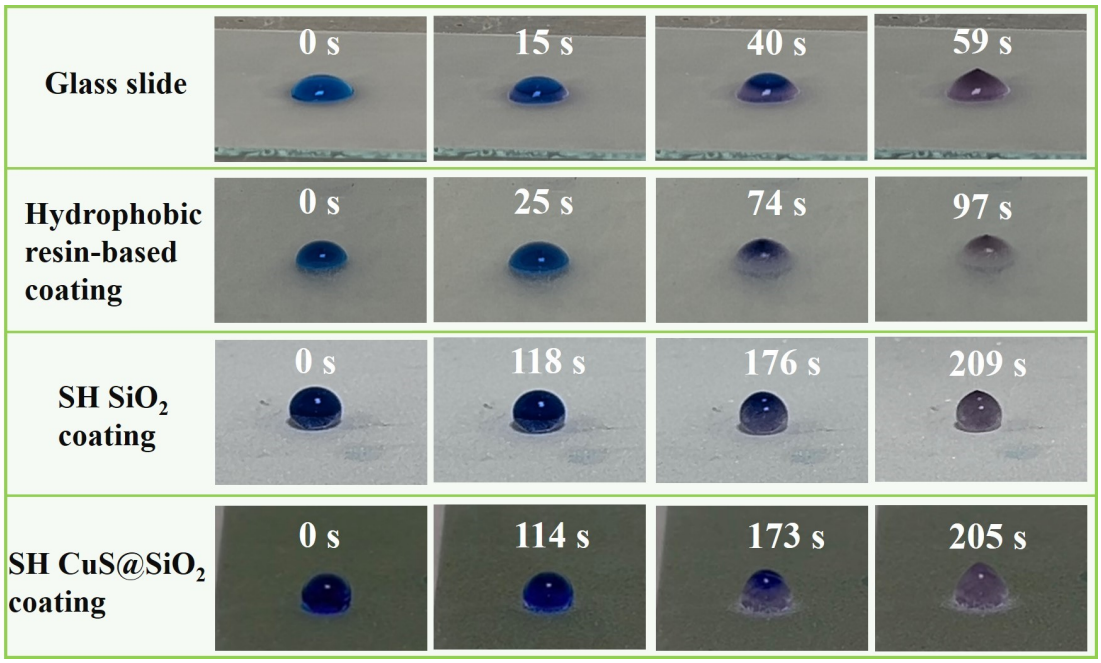

Fig. S11. Photographs during water droplet freezing on glass slide and various coatings at -35°C without light illumination.

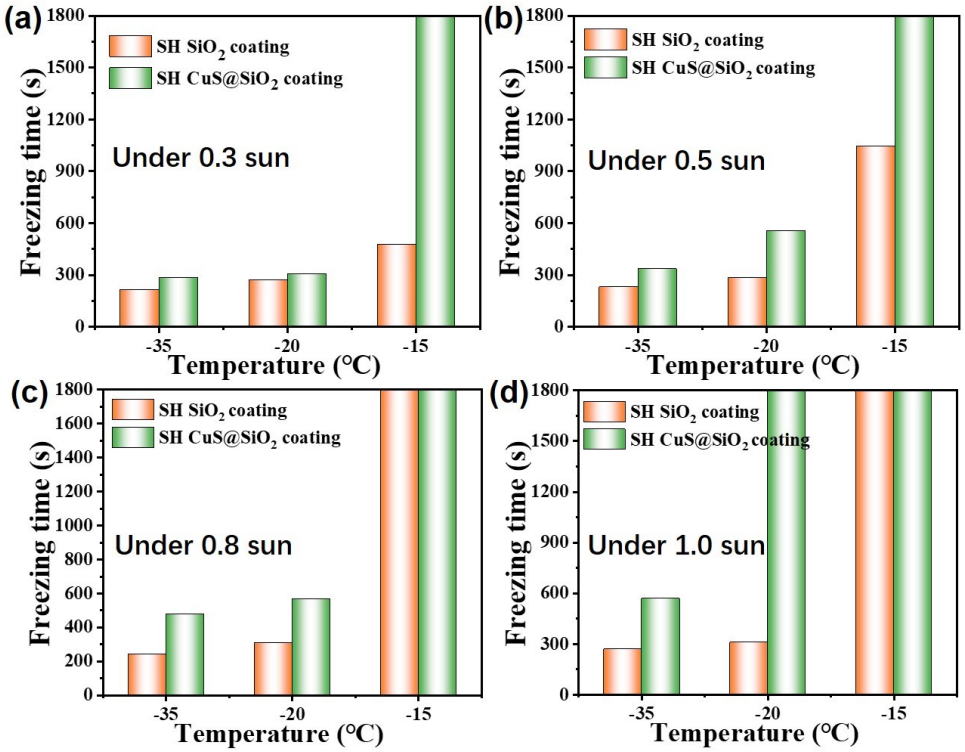

Fig. S12. Freezing time for the typical SH SiO_2 coating and SH photothermal CuS@SiO_2 coating, at -35°C, -20°C and -15°C, respectively, under different solar power intensity.

References

1. Z. Yang, N. Wei, N. Xue, R. Xu, E. Yang, F. Wang, H. Zhu and H. Cui, *J. Colloid Interface Sci.*, 2024, **656**, 189-199.
2. Y. Xie, G. Bertoni, A. Riedinger, A. Sathya, M. Prato, S. Marras, R. Tu, T. Pellegrino and L. Manna, *Chem. Mater.*, 2015, **27**, 7531-7537.
3. Y. Xie, L. Carbone, C. Nobile, V. Grillo, S. D'Agostino, F. Della Sala, C. Giannini, D. Altamura, C. Oelsner, C. Kryschi and P. D. Cozzoli, *ACS Appl. Nano Mater.*, 2013, **7**, 7352-7369.
4. Y. Xie, W. Chen, G. Bertoni, I. Kriegel, M. Xiong, N. Li, M. Prato, A. Riedinger, A. Sathya and L. Manna, *Chem. Mater.*, 2017, **29**, 1716-1723.
5. B. Wang, T. Wang, S. Ma, J. Bai and H. Ma, *J. Colloid Interface Sci.*, 2024, **660**, 192-202.
6. A. Zhang, K. Wang, M. J. Nine, M. Cao, H. Zong, Z. Liu, H. Guo, J. Liu and D. Losic, *Green Energy Environ.*, 2024, **9**, 378-389.
7. J. Yang, Y. Chen, X. Jia, Y. Li, S. Wang and H. Song, *ACS Appl. Mater. Interfaces*, 2020, **12**, 47029-47037.
8. K. Wang, Z. Cheng, P. Li, Y. Zheng, Z. Liu, L. Cui, J. Xu and J. Liu, *J. Colloid. Interf. Sci.*, 2021, **581**, 504-513.
9. X. Zhao, X.-J. Zha, L.-S. Tang, J.-H. Pu, K. Ke, R.-Y. Bao, Z.-y. Liu, M.-B. Yang and W. Yang, *Nano Research*, 2020, **13**, 255-264.
10. Z. Yang, N. Wei, N. Xue, R. Xu, E. Yang, F. Wang, H. Zhu and H. Cui, *Journal of Colloid and Interface Science*, 2024, **656**, 189-199.
11. X. Zhang, J. Liu, S. Han, W. Li, C. Li, F.-L. Gao, C. Shu, Z.-Z. Yu and X. Li, *ACS Applied Materials & Interfaces*, 2023, **15**, 51289-51299.
12. R. Xu, H. Cui, N. Wei, J. Zhao, X. Song, Y. Han, J. Yang, A. Wang and M. Zhao, *Desalination*, 2024, **570**, 117094.
13. H.-S. Kang, J.-W. Zou, Y. Liu, L. Ma, J.-R. Feng, Z.-Y. Yu, X.-B. Chen, S.-J. Ding, L. Zhou and Q.-Q. Wang, *Adv. Funct. Mater.*, 2023, **33**, 2303911.
14. Q. Wang, L. Wang, S. Song, Y. Li, F. Jia, T. Feng and N. Hu, *Desalination*, 2022, **525**, 115483.
15. X. Chen, S. He, M. M. Falinski, Y. Wang, T. Li, S. Zheng, D. Sun, J. Dai, Y. Bian, X. Zhu, J. Jiang, L. Hu and Z. J. Ren, *Energy Environ. Sci.*, 2021, **14**, 5347-5357.
16. C. Chang, M. Liu, L. Li, G. Chen, L. Pei, Z. Wang and Y. Ji, *J. Mater. Res.*, 2022, **37**, 294-303.
17. Z. Liu, F. Wu, T. Lv, Y. Qu, Z. Zhang, C. Yu, C. Zhao and G. Xing, *Desalination*, 2024, **573**, 117207.
18. X. Ming, A. Guo, Q. Zhang, Z. Guo, F. Yu, B. Hou, Y. Wang, K. P. Homewood and X. Wang, *Carbon*, 2020, **167**, 285-295.
19. K. Wang, Z. Cheng, P. Li, Y. Zheng, Z. Liu, L. Cui, J. Xu and J. Liu, *Journal of Colloid and Interface Science*, 2021, **581**, 504-513.
20. Y. Yang, H. Zhao, Z. Yin, J. Zhao, X. Yin, N. Li, D. Yin, Y. Li, B. Lei, Y. Du and W. Que, *Mater. Horiz.*, 2018, **5**, 1143-1150.